A Novel Defined Pyroptosis-Related Gene Prognostic Index for Clear Cell Renal Cell Carcinoma

xuexiang Li
Wuhan Union Hospital
Yarong Song
Wuhan Union Hospital
Bing Liu
Wuhan Union Hospital
Liang Chen
Wuhan Union Hospital
dingheng Lu
Wuhan Union Hospital
Yunxue Li
Wuhan Union Hospital
Lulin Cheng
Wuhan Union Hospital
Fang Lyu
Wuhan Union Hospital
Pu Zhang
Wuhan Union Hospital
yifei xing (yfxing@hust.edu.cn)
Wuhan Union Hospital https://orcid.org/0000-0002-5303-9633

Research article

Keywords: Bioinformatics, Clear cell renal cell carcinoma, Pyroptosis-related genes, Prognostic model, Risk score

Posted Date: September 30th, 2021

DOI: https://doi.org/10.21203/rs.3.rs-919283/v1

Abstract

Background: Clear cell renal cell carcinoma (ccRCC), a common pathological subtype of renal cancer with high aggressiveness, has been reported to be associated with chronic inflammation. Pyroptosis, a newly discovered inflammatory form of programmed cell death, can aggravate the inflammatory response. However, the influence of pyroptosis-related genes on ccRCC patient outcomes is yet unknown.

Methods: In this study, 43 differentially expressed pyroptosis-related hub genes were identified by analysing The Cancer Genome Atlas–Kidney Renal Clear Cell Carcinoma dataset. The risk-score model was selected using the least absolute shrinkage and selection operator Cox regression and Cox multivariate methods, and all patients were divided into two risk subgroups based on the risk score. Prognostic value of the risk-score model was verified through survival curve, receiver operating characteristic curve and risk curve. Gene ontology and Kyoto Encyclopaedia of Genes and Genomes analyses suggested that the differentially expressed genes between the two subgroups were enriched in immune-mediated categories. Furthermore, the relationship between the risk-score model and ESTIMATE immune score and immunophenoscore was analysed. Finally, Nomogram was constructed based on the results of cox regression analyses.

Results: The training cohort and the validation cohort enrolled 346 and 148 ccRCC patients respectively. The risk-score model was constructed by two genes (*AIM2* and *GSDMB*). The area under curve of the ROC curve in two cohorts were both greater than 0.6. The grade and risk score were selected as independent factors and used to construct a nomogram to predict ccRCC patients' survival rate with the c-index of 0.68. Moreover, high-risk score subgroup was associated with a higher immune score and a lower percentage of *PBRM1* mutations. The risk score was positively related to the degree of immune infiltration of CD8+ T, T follicular helper, gamma delta T, and regulatory T cells, and patients with a higher risk score were more likely to benefit from immune checkpoint inhibitor therapy.

Conclusion: The risk-score model based on pyroptosis-related genes constructed in our study is a promising biomarker to predict the prognosis, molecular and immune characteristics, and immune benefit from immune checkpoint inhibitor therapy in ccRCC patients.

Introduction

Renal cell carcinoma (RCC) is one of the most challenging urological cancers, and its incidence is rapidly increasing worldwide(Siegel, Miller 2018). RCC is a heterogeneous disease encompassing many histopathological subtypes, with clear cell RCC (ccRCC) being the most frequent, accounting for more than 80% of cases and being the primary cause of cancer death(Linehan 2012). Small molecular targeted drugs such as tyrosine kinase inhibitors have been accepted as first-line therapy in advanced RCC(Barata, De Liano 2018), but a highly adaptive and heterogeneous tumour microenvironment (TME) facilitates the development of drug resistance. Immune checkpoint inhibitors (ICIs) are promising therapeutics that block negative regulatory immune signals to activate anti-tumour immune responses in patients.

Nevertheless, its utility remains limited, as the majority of cancer patients have no expected response to ICI therapy. Interestingly, compared to most other cancers which respond to anti-PD1 therapy, ccRCC has only a modest mutation burden(Lawrence, Stojanov 2013). Moreover, the extensive infiltration of CD8+ T cells in ccRCC has been previously proven to be related to worse outcomes which is inconsistent with most other cancers(Fridman, Zitvogel 2017). Considering the paradoxical limitations of ccRCC treatments, we need to explore new therapeutic targets associated with ICI to improve the clinical prognosis of ccRCC. Therefore, a feasible and reliable novel prognostic model is needed to implement targeted therapies.

Pyroptosis is an inflammation-dependent programmed cell death that is mediated by the gasdermin superfamily(Kovacs and Miao 2017, Shi, Zhao 2015). The gasdermin superfamily contains gasdermin A/B/C/D/E (GSDMA/B/C/D/E) and DFNB59 (Pejvakin) in humans(Ding, Wang 2016) (He, Wan 2015). Except for Pejvakin, all of the above molecules are composed of an N-terminal pore-forming domain and a C-terminal repressor domain(Rogers, Erkes 2019, Kuang, Zheng 2017, Liu, Wang 2019). Activation of the N-terminal pore-forming domain by caspases or granzymes can cause pyroptosis, which is not detectable in Pejvakin(Rogers, Fernandes-Alnemri 2017). The N-terminal domain can form pores (1–2 μm in diameter) in the plasma membrane by oligomerization, allowing mature IL-1β/IL-18 and caspase-1 to pass through(Ding, Wang 2016). Then, the cell swells and ruptures as water enters through the pores, accompanied by the release of IL-1β and IL-18(Fink and Cookson 2006). Increasing evidence has confirmed the vital role of pyroptosis in tumours. However, the specific regulatory mechanisms in ccRCC have not been clearly elucidated. It has been reported that tumorigenesis, invasion, and metastasis are associated with inflammatory complexes(Qian and Pollard 2010), proinflammatory cytokines, and gasdermin proteins(Kolb, Liu 2014), which are key components of pyroptosis. Studies have demonstrated that high levels of GSDMB and GSDMC are related to poor survival in breast cancer(Hou, Zhao 2020), and that enhanced expression of the GSDMB results in a worse feedback to HER-2-targeted therapy(Hergueta-Redondo, Sarrio 2014). Overexpression of GSDMC enhances colorectal cancer cell multiplication and angiogenesis[19]. Conversely, the downregulation of GSDMC significantly reduced the proliferation of colorectal cancer(Miguchi, Hinoi 2016). Pyroptosis may play a crucial role in the development of multiple tumours, however, its specific function in ccRCC has rarely been investigated. In this study, we obtained pyroptosis-related genes through a systematic review of pyroptosis-related studies and identified the expression of related genes between cancerous and normal renal tissues. The results suggest correlations among pyroptosis, the tumour immune microenvironment, and the ICI strategy.

Materials And Methods

Datasets

Data source and pre-processing: We obtained the related RNA-sequencing (RNA-seq) dataset and corresponding clinical information from The Cancer Genome Atlas–Kidney Renal Clear Cell Carcinoma dataset (https://portal.gdc.cancer.gov/). All level 3 tumour RNASeqV2 mRNA expression datasets of 543

ccRCC tissues and 72 adjacent normal kidney tissues were obtained from TCGA (April 15, 2021). Inclusion criteria were listed as follows: (i) ccRCC confirmed through pathologic evidence; (ii) complete mRNA expression data and corresponding survival information; (iii) OS were above 30 days. Lastly, 494 patients with ccRCC and with the corresponding clinical-pathological data, including sex, age, tumour T stage, M stage, TNM stage and histologic grade and OS were included for further analysis. With the help of caret package, these 494 patients were stochastically split into two sets: 70% for training set (346 patients) and 30% validation set (148 patients). Comparison of baseline clinical characteristics of the two cohorts was shown in **Table S1(Additional file 1)**.

Pyroptosis-related genes detection

After consulting published literatures[20-26], we selected 51 pyroptosis-related genes as presented in **Table S2(Additional file 2)**. A total of 43 pyroptosis-related genes were identified through mining available mRNA expression data of ccRCC from TCGA. Transcriptional counts were transformed to Transcripts Per Million (TPM) values as the official instruction provided. We identified DEGs with the assistance of the "EdgeR" package and the criteria of DEGs were as follows: p value< 0.05, |log2FoldChange| > 1. DEGs are notated as follows: * means P < 0.05, ** means P < 0.01, and *** means P <0.001, **** means P <0.0001.

Bioinformatics analysis

To elucidate the biological functions of these 43 pyroptosis-related genes in ccRCC, we performed the "ConsensusClusterPlus" package (1,000 iterations and resample rate of 80%, http://www.bioconductor.org/) and divided the patients into clusters. A principal component analysis (PCA) was performed using R version 4.0.3 and plotted using the "ggplot" package to evaluate gene-expression patterns in different subgroups. We utilized Search Tool for the Retrieval of Interacting Genes (STRING)[47], version 11.0 (https://string-db.org/) to build up a PPI network of the DEGs, The immunoscore of ccRCC patients was calculated by R package "ESTIMATE" and the fraction of 22 types of immune cells was estimated from gene expression data by CIBERSORT algorithm to explore the relationship between the risk subgroups and immune cell infiltration (CIBERSORT; https://cibersort.stanford.edu/). The samples adopted according to p < 0.05 with 1,000 permutations were included for subsequent comparing of immune infiltration levels.

Development and validation of pyroptosis-related genes prognostic model

To further assess the precise prognostic value of pyroptosis-related genes, the least absolute shrinkage and selection operator regression analysis was performed on the basis of the expression of 43 pyroptosis-related genes in the TCGA training cohort. Then we performed univariate and multivariate Cox analysis and retained their coefficients (**Additional file 3: Table S3**). To avoid omissions, we set 0.2 and 0.05 as the cut-off P-value for univariate and multivariate Cox analysis separately. Ultimately, we obtained two genes and the risk scores were calculated after centralization and standardization of the TCGA expression data, and the formula of the risk score was constructed as follows: Risk Score = expression of gene1 ´ β1 + expression of gene2 ´ β2. According to the individual risk scores, all patients

were distributed into one of two subgroups (low and high) demarcated by the median risk score and survival curves were estimated by the Kaplan–Meier method. We plot a 1-,3- and 5-year receiver operating characteristic curve through using R packages “survival” and “survminer”. Survival predication based on gene expression was performed using the GEPIA database (http://gepia.cancer-pku.cn/).

Functional enrichment analysis

GO enrichment and KEGG pathway analyses were carried out to predict the potential biological processes, cellular components, and molecular functions of different subgroups. IPS analysis was conducted on the basis of a web-based database, The Cancer Immunome Atlas (TCIA, https://tcia.at/home)

Nomogram establishment and validation for prognostic risk prediction

Risk score and grade, as independent prognostic factors were incorporated into the nomogram model in estimation of the 1-, 3-, and 5-year survival probability. We then assessed both discrimination and calibration in the independent validation samples. The nomogram was validated with 1000 bootstrap resamples to calculate a robust concordance index (C-index). The C-index value was between 0.5-1.0. 1.0 suggests the model has a perfect capacity for accurately distinguishing outcomes, and 0.5 suggests random chance. The calibration curves were made by plotting the observed rates against the predicted probabilities of the nomogram. Overlap with the reference line showed perfect consistency of the model.

Human ccRCC tumour samples

A total of 12 paired ccRCC tissues and corresponding normal tissue samples were obtained from ccRCC patients. All human specimens were studied after approval by the Human Research Ethics Committee of Huazhong University of Science and Technology.

RNA Extraction and quantitative real-time PCR

Total RNA was extracted from ccRCC samples and adjacent normal samples with TRIzol reagent (Invitrogen, USA). HiScript II Q RT SuperMix for qPCR (Vazyme, China) was used to synthesize cDNA. After that, cDNA samples were used for quantitative real-time PCR with technical duplicates. The primer sequences are available below:

5'-β-actin,5'-GTGGGGCGCCCCAGGCACCA-3'

3'-β-actin,5'-CTCCTTAATGTCACGCACGATTTC-3'

5'-GSDMB, 5'-TCACCCTGATGGACATTCTGGAC-3'

3'-GSDMB, 5'-TGATGGTGGAAGCCCTGGAAA-3'

5'-AIM2, 5'-CCCGAAGATCAACACGCTTCA-3'

3'-AIM2, 5'-TCATTGTGTCCTCGTTTCTAACCC-3'

Statistical Analysis

We used R version 4.0.3, and GraphPad Prism 8.0 to perform statistical analysis.

We performed a Wilcox test over the expression values of the pyroptosis-related genes in tumour versus adjacent normal tissues. Student's t-test to compare two subgroups and more than two subgroups. For comparisons of baseline characteristics between groups, we applied chi-square tests on categorical variables and t-tests on continuous variables. Survival curves analysis were made using Kaplan–Meier method, and the log-rank test was applied for comparison. The expression correlation among subgroups, clinicopathological features, risk scores, immunoscores was investigated by Spearman's correlation analysis. For univariate and multivariate analysis, a Cox proportional hazard regression model was used to determine the independent prognostic value of risk scores integrated with other clinical parameters. $p < 0.05$ indicated statistical significance.

Results

Expression of pyroptosis-related genes was upregulated in ccRCC

With the aim of elucidating the role of pyroptosis-related genes in the course of ccRCC, we first identified 51 such genes by reviewing published literatureKarki and Kanneganti 2019, Xia, Wang 2019, Man and Kanneganti 2015, Ruhl, Shkarina 2018, Hu, Chen 2020, Zhou, Zhang 2018, Tan, Huang 2020), overlapped them with differentially expressed genes (DEGs) obtained from gene profiles of 71 sets of paired samples in TCGA database, and acquired an intersection set of 43 genes ($p < 0.01$; **Figure 1A**). Further, we measured their expression in 71 sets of paired samples and found that 37 genes (VPS4A, CASP5, CHMP6, CASP1, IL18, GPX4, CHMP2A, IRF2, CASP4, HMGB1, NLRC4, IRF1, PLCG1, NLRP6, NLRP7, GSDMC, CASP3, NOD1, AIM2, GSDMD, CASP6, GSDMA, IL1A, GZMB, GSDMB, NLRP1, TIRAP, PRKACA, IL1B, NOD2, PYCARD, CHMP4A, NLRP3, CASP8, CHMP4B, SCAF11, and BAX) were upregulated in tumour tissues, and six other genes (CHMP2B, DFNB59, PLCG2, CYCS, NLRP2, and TP63) were downregulated in tumour tissues. Further, we intended to clarify the interplay of selected genes through protein–protein interaction (PPI) analysis, as presented in **Figure 1B**. We set the highest confidence at 0.9 of interaction score for PPI analysis. **Figure 1C** depicts the correlation network containing all pyroptosis-associated genes. The results reveal the biological role of pyroptosis-related genes in ccRCC development.

Consensus clustering for pyroptosis-related genes with the characteristics and survival of patients with ccRCC

Further, to investigate the relationship between the expression level of pyroptosis-related genes and clinical characteristics, we conducted a consensus clustering analysis. After testing the clustering potency according to the similarity displayed by the expression levels of DEGs and the proportion of ambiguous clustering measures by setting k from 2 to 9, k = 2 was identified as optimal clustering stability (**Figure 2A- B**). Thereafter, patients were divided into two clusters; cluster 1 (n = 142) and cluster 2 (n = 352). The gene expression profiles and clinical characteristics of patients are presented in a heatmap

(**Figure 2C**). The individual gene expression profiles and the clinical characteristics including survival status (alive or dead), degree of tumour differentiation (G1–G4), tumour-node-metastasis (TNM) stage, M stage, T stage, age (<60 or ≥60 years), and sex are shown in the heatmap; differences in clinical features between clusters are insignificant. Overall survival (OS) between clusters was not significant (p = 0.394; **Figure 2D**).

Development and validation of a risk-score prognostic model in TCGA cohort

Further, we attempted to determine the prognostic value of pyroptosis-related genes in ccRCC patients. The 494 patients were randomly distributed in the TCGA training cohort with a validation cohort in the ratio of 7:3. All clinical characteristics including age, sex, T stage, M stage, grade, and TNM stage were found to have no statistical significance between the two cohorts (all p > 0.05, **Table S1**). To construct a more accurate prediction model of clinical outcome correlated with pyroptosis-related genes, we conducted the least absolute shrinkage and selection operator regression analysis on 43 DEGs based on the TCGA training cohort and selected six genes (AIM2, BAX, GSDMB, NLRP6, SCAF11, TIRAP; **Figure 3A-B**). Cox univariate analysis was performed on these six genes, and five variates (those with p < 0.2) were subjected to the Cox multivariate analysis, giving a coefficient to each variate. AIM2 and GSDMB were linked to an increased risk (HRs > 1), whereas NLRP6, SCAF11, and TIRAP may be protective genes (HRs < 1). The results of all Cox univariate and multivariate analyses are shown in **Table S3**. Using the coefficient of the final two variables, we constructed a two-gene risk score model. The risk score of each patient was calculated using the following equation: risk score = (1.035 ´ AIM exp) + (1.091 × GSDMB exp). We then split the TCGA training and validation cohorts into two groups (high and low) from the median risk score of the TCGA training cohort. Risk score, immunoscore, grade, TNM stage, M stage, N stage, age, and sex are presented in a heatmap (**Figure 3C**), which displays the upregulation of AIM2 and GSDMB in the high-risk score group. The distribution of the risk score, OS, OS status, and expression profiles of the two-gene risk-score model in TCGA training and validation cohorts are displayed in **Figures 3D and 3E**. Low-risk groups in both the training and validation cohorts were associated with a better OS (p < 0.001, **Figure 3F–G**). In an attempt to test the prognosis accuracy of this two-gene model, we carried out 1-, 3-, and 5-year receiver operating characteristic curve analyses by comparing the respective area under curve (AUC) values. In the TCGA training cohort, the 1-, 3- and 5-year AUC values for the two-gene risk-score model were 0.680, 0.626, and 0.675, respectively (**Figure 3H**). In the TCGA validation cohort, they were 0.661, 0.644, and 0.657, respectively (**Figure 3I**). The AUC values showed that the two-gene risk score model had a satisfactory discrimination potential for ccRCC patients. These results demonstrate that the two-gene risk-score model is a potent predictor of ccRCC prognosis.

Prognostic risk scores correlated with immunoscore and PBRM1 mutation in ccRCC

The correlation between risk score and clinical characteristics was further studied. We identified DEGs between high and low-risk subgroups in TCGA training and validation cohorts separately using Wilcox test with a threshold of p value 0.05 and |log2FoldChange|≥1, and obtained an intersection set of 1126 genes. Among them, 1095 were upregulated in the high-risk score subgroup and 31 were downregulated

(**Figure 4A; Additional file 4: Table S4**). DEGs were then subjected to GO and KEGG analysis, and were found to be enriched and regulates T cell activation and primary immunodeficiency (**Figure 4B**). This led us to further examine the immunoreactive differences between the high-and low-risk subgroups. Hence, we compared the immunoscore of the two groups and found that the immunoscore of the low-risk subgroup was distinctly lower than that of the high-risk subgroup ($p < 0.0001$, **Figure 4D**). Contrary to other cancers, a higher immunoscore represents more infiltration of immune cells in the tumor microenvironment and a better prognosis. However, in the case of ccRCC, higher immunoscores are associated with a worse prognosis. To better explain this phenomenon, we compared PBRMI mutation differences between high- and low-risk subgroups based on the available literature(Braun, Hou 2020). We compared the mutations in TCGA training cohorts and found that the percentage of patients with PBRM1 mutation in the low-risk subgroup was distinctly higher than that in the high-risk subgroup (Chi-square $p < 0.001$, **Figure 4C, 4E**)

Relationships between risk scores and infiltration abundances of nine immune cell types

We then determined the differences in the immune microenvironment between the two groups. We used the CIBERSORT algorithms to calculate the infiltrating levels of 22 immune cell types in TCGA training cohort, with $p < 0.05$, as the threshold. Moreover, the proportion of the eight immune cell types was significantly different in different subgroups (**Figure 5A**). The results show that risk scores are negatively related to proportions of CD4+ T memory resting cell, macrophages M0, macrophages M2, mast resting, and naive B cells, and positively related to CD8+ T, T follicular helper, gamma delta T, and regulatory T cells (**Figure 5B-J**). Such evidence suggests that our risk-score model based on pyroptosis-related genes is related to the immune microenvironment of ccRCC. Utilising the Tumour Immune Estimation Resource database, we demonstrated the correlation between two hub genes (AIM2 and GSDMB), tumour purity, and five infiltrating immune cells. Expression of AIM2 and GSDMB was negatively correlated with tumour purity (Spearman rho = -0.284 and -0.04, respectively; all $p < 0.001$), positively related to infiltrating regulatory T cells, T follicular helper cells, and CD8+ T cells, and negatively related to CD4+ T cells and B naive cells (all $p < 0.05$). The above results demonstrate that immune infiltration plays a major role in ccRCC development.

Risk score-based treatment strategy for ccRCC

We analysed the expression levels of four types of immune checkpoint molecules, including CTLA4, PD1, PD-L1, and PD-L2, between two subgroups of different risk scores. The high-risk subgroup was proved to possess higher expression of immune checkpoint molecules (**Figure 6A**), and the risk scores were positively correlated with the expression of immune checkpoint molecules (**Figure 6B**). In addition, we used the Cancer Immunome Atlas (TCIA)-recommended immunophenoscore (IPS) scheme to evaluate the immunogenicity of the two groups. Ips_ctla4_neg_pd1_pos, Ips_ctla4_pos_pd1_neg, and Ips_ctla4_pos_pd1_pos reached higher scores in the high-risk group (**Figure 6C**). These results might indicate a potentially better response to immunotherapy among patients in the high-risk group.

Expression validation of the two hub genes by quantitative real-time PCR

To better describe the expression levels of two hub genes in cancerous and normal renal tissues, we collected 12 normal renal samples and 12 ccRCC samples. Compared to normal tissues, the expression levels of AIM2 and GSDMB were increased in tumour samples (**Figure 7 A-B**, all $p < 0.05$). Moreover, a higher expression of GSDMB and AIM2 was associated with a poor prognosis (HR = 1.6 and 1.7, respectively; all $p < 0.01$)

Independent prognostic value of the risk score model and development of a predictive nomogram in TCGA cohort

We set out to test the qualification of our two-gene risk-score model in the prediction of ccRCC patient prognosis by univariate and multivariate Cox regression analysis in TCGA training cohorts, judging from the hazard ratios (HR) and the 95% confidence intervals (CI) of the risk score, both analyses demonstrated our model's decent prognostic efficiency independent of clinical characteristics including sex, age, TNM stage, and grade. The HRs of the two analyses were 2.074 95% CI: 1.413–3.044 ($p < 0.001$) and 1.752 95% CI: 1.018–2.599 ($p < 0.01$; **Figure 8A and 8B**). All Cox univariate and multivariate analysis results of TCGA validation cohorts are shown in **Figure S1(Additional File 5)**. To complement the prognostic model, we constructed a nomogram to predict ccRCC prognosis based on Cox regression analysis of TCGA training cohort. Our nomogram considered two predictive factors: pathologic grade and prognostic model (**Figure 8C**). Each variate was graded based on a multivariate Cox regression analysis. The overall nomogram score was the sum of the individual scores of all the predictive variables. Higher nomogram scores indicate worse 1-, 3-, and 5-year survival rates and vice versa (**Figure 8D–F**). The C-index of the nomogram for prediction was 0.68 (95% CI: 0.656–0.704) and a calibration plot in fine consistency with the ideal curve proved our nomogram to be stable in predicting the clinical prognosis of ccRCC patients.

Discussion

Pyroptosis is a double-edged sword for tumours. Apart from repressing tumour cell growth, pyroptosis also forms a microenvironment that could be beneficial for the growth and proliferation of tumor cells(Kolb, Liu 2014). As a form of inflammatory and programmed cell death, pyroptosis has long been believed to be linked to caspase-1 induced monocyte death(Cookson and Brennan 2001, Bergsbaken, Fink 2009). According to recent reports, the activation of caspase-1 or caspase-4/5/11 and gasdermin D plays a central role during this process. Multiple genes are involved in the regulation of pyroptosis, but whether they are associated with tumour progression is unclear. Furthermore, the role of pyroptosis in ccRCC had not been elucidated.

In the present study, we first obtained 51 pyroptosis-related genes by reviewing published literature, and used least absolute shrinkage and selection operator Cox regression and Cox univariate analysis to identify six pyroptosis-related hub genes affecting patient OS in ccRCC. Furthermore, we constructed a risk-score model based on two genes (AIM2 and GSDMB), which are independent prognostic factors for poor outcome of ccRCC. The risk-score model was proven to be a valid prognostic immune-related

biomarker for ccRCC, with better survival in patients in the low-risk group and worse survival in patients in the high-risk group in both the training and validation cohorts sourced from TCGA. Furthermore, univariate and multivariate Cox regression analyses proved that the risk score was an independent prognostic factor for patients with ccRCC. A nomogram, including pathological stage and risk scores, serves as a statistical tool to predict OS in patients with ccRCC. Calibration plots demonstrated optimal agreement between the actual and predicted prognoses, guaranteeing the reliability and repeatability of the nomogram.

Absent in melanoma 2 (AIM2) is a member of the ALR (AIM2-like receptors) family and consists of an N-terminal pyrin domain and a C-terminal hematopoietic, interferon-inducible, and nuclear localisation domain. It is located in the cytoplasm, where it can sense DNA in the cytosol as well as self-dsDNA(Man and Kanneganti 2015). Activation of AIM2 initiates assembly of the AIM2 inflammasome complex and leads to apoptosis-associated speck-like protein containing a caspase recruitment domain oligomerization as well as recruitment of pro-caspase-1(Kumari, Russo 2020). The pro- or anti-cancerous roles of AIM2 have been shown to vary according to tumour type. For instance, AIM2 performs a pro-tumorigenic role in skin carcinomas(de Koning, van Vlijmen-Willems 2014) and is anti-cancerous in BRAF-mutant colorectal cancer cells (Shah, Qin 2021). Higher levels of AIM2 protein were observed in non–small cell lung cancer patients and correlated with worse prognosis(Qi, Dai 2020). However, low expression of AIM2 resulted in worse overall and disease-free survival in HBV-infected patients with hepatocellular carcinoma patients(Chen, Liu 2017). In the present study, AIM2 was upregulated in ccRCC tissues compared to that in pericarcinomatous tissues, and high AIM2 expression predicted worse prognosis.

Gasdermin B (GSDMB) belongs to the gasdermin family which has regulatory functions in cell proliferation, differentiation, and pyroptosis. GSDMB participates in pyroptosis via the classical pathway (caspase 1) and the non-canonical pathway (caspase 4)(Panganiban, Sun 2018, Chen, Shi 2019). GSDMB overexpression is related to increased migration capability and resistance to anti-HER2 therapies in human epidermal growth factor receptor 2-positive breast cancer(Molina-Crespo, Cadete 2019). Most gastric cancerous samples showed augmented GSDMB expression in comparison with normal samples(Komiyama, Aoki 2010). Moreover, higher levels of GSDMB protein were observed in uterine cervical cancer tissues compared to adjacent tissues, and GSDMB overexpression promoted the growth of cervical cancer cell(Sun, Yang 2008). In our study, high GSDMB expression predicted a shorter overall survival, indicating that GSDMB might be a cancer-promoting gene in ccRCC. However, these findings have produced conflicting results with the participation of GSDMB in pyroptosis. A possible reason for this discrepancy may be that pyroptosis may not occur in all tumour cells, and the role of GSDMB in ccRCC requires further investigation. The coefficients of AIM2 and GSDMB were positive in the calculation formula of the risk-score model. Therefore, there was a positive relationship between the risk score and AIM2 and GSDMB scores.

Pyroptosis, as an inflammatory programmed cell death, activates multiple signalling pathways and releases many inflammatory factors, such as IL1B/IL-18, and is closely related to immune

responses(Zhou and Fang 2019). To gain further biological insights into the immunological nature of the risk score model subgroups, we obtained overlapping DEGs in TCGA training and validation cohorts. By analysing the DEGs between distinct risk subgroups, we discovered that these genes were mostly considered to be related to lymphocyte differentiation, activation and regulation of T cell and primary immunodeficiency. According to our results from GO and KEGG analyses, we made a reliable assumption that pyroptosis may alter the components of the immune cells in TME. Then we calculated immunoscores in different risk groups based on “estimate” R package. Surprisingly, immunoscores in the high-risk subgroup were evidently higher than those in the other subgroups.

TME, an active operative system connected by intercellular communications, is liable for tumour progression and metastasis, and its heterogeneity can affect patient prognosis and therapeutic response. For multiple tumours, higher levels of tumor-infiltrating lymphocytes and immunoscores are associated with a better outcome(Fridman, Zitvogel 2017). Gene alterations may affect the formation and phagocytic function of immune cells to exert the immunomodulatory effect, among which missense variations were the most common, followed by nonsense variation and frameshift deletions(Ma, Yang 2001). In agreement with prior studies, high PBRM1 mutations were related to higher angiogenesis gene expression(Hakimi, Voss 2019), which was associated with improved response, progression-free survival, and OS with PD-1 blockade(Braun, Hou 2020). In our study, the low-risk subgroup with high PBRM1 mutations had a better outcome than the high risk-score subgroup with high PBRM1 mutation.

Next, we explored the relationship between the risk-score model and known predictive biomarkers for immunotherapy, including CTLA4, PD1, PD-L1, and PD-L2. Interestingly, we found that high-risk subgroups were accompanied by higher CTLA4, PD-1, PD-L1, and PD-L2 expression, and that risk scores were strongly positively correlated with expression of CTLA4 and moderate positive correlation with PD1, PD-L1, and PD-L2. Moreover, based on the TCIA databases, targeted treatment had a better effect in the high-risk subgroup. Understanding the landscape of the TME could help in finding new ways to treat ccRCC or alter the TME to improve the effectiveness of immunotherapies. The proportions of some immune cells differed between the subgroups. While cytotoxic CD8 + T, T follicular helper, Treg, and T gamma delta cells tended to be enriched in the high-risk score subgroup, CD4 + T memory resting, M0, M2, and resting mast cells were common in the low risk-score subgroup. A substantial body of research has revealed that dense infiltration of T cells, especially cytotoxic CD8 T cells, indicates a worse prognosis in ccRCC(Fridman, Zitvogel 2017).

T cell activation, as an indicator of immunotherapy response, is a core component of ccRCC(Hah and Koo 2021). In contrast to other malignancies, ccRCC is characterised by the highest T cell and immune infiltration(Hah and Koo 2021). However, an environment with abundant Th2 and regulatory T cells suppresses the immune response and is related to the tumour mutation load, which is associated with poor prognosis(Senbabaoglu, Gejman 2016). Although the difference between risk-score models was not significant, considering the important role of regulatory T cells, we found that the proportion of regulatory T cells was positively correlated with risk scores, which might suppress the immune response.

Our study had several limitations. First, although the internal validation of our results may help to generalise our findings, the cohorts in this study were constructed only from TCGA datasets. Second, the lack of external validation data limited further exploration between the TME and the risk-score model. Therefore, these findings should be considered tentative, and further investigation in larger cohorts is needed to validate these approaches. Additionally, further understanding of the regulatory mechanisms of pyroptosis and deeper identification of relevant pathways/targets in ccRCC should pave the way for precision immunotherapy. A workflow chart for the present study is provided in Fig. 9.

Conclusions

The risk-score model based on two genes is a promising immune-related prognostic biomarker. The risk-score model grouping may help in distinguishing immune and molecular characteristics and predicting patient outcomes. The risk-score model might be a potential prognostic indicator of immunotherapy, but further studies are needed to clarify this point.

Abbreviations

ccRCC: Clear cell renal cell carcinoma

ROC curve: Receiver operating characteristic curve

GO: Gene ontology

KEGG: Kyoto Encyclopaedia of Genes and Genomes

AUC: Rrea under curve

TME: Tumour microenvironment

ICIs: Immune checkpoint inhibitors

TCGA: The genomic data commons data portal and the cancer genome atlas database

DEGs: Differentially expressed genes

PPI: Protein–protein interaction

TNM: Tumour-node-metastasis

OS: Overall survival

HR: Hazard ratio

IPS: Immunophenoscore

CI: Confidence intervals

Lasso: Least absolute shrinkage and selection operator

BP: Biological process

CC: Cellular component

MF: Molecular function

Declarations

Acknowledgements:

We would like to acknowledge the TCGA for providing data.

Authors' contributions:

YX, XL: The conception and design of the study. LB, PZ: The acquisition of data. XL, DL, LC, YL: Analysis and interpretation of data. XL, YS, FL, LLC: Drafting the article or revising it critically for important intellectual content. All authors read and approved the final paper.

Funding:

This work was supported by the National Natural Science Foundation of China (Grants 81272847 and 81772751).

Availability of data and materials:

The datasets used and/or analysed during the current study are available from the corresponding author on reasonable request.

Ethics approval and consent to participate:

All procedures performed in studies involving human participants were in accordance with the ethical standards of Union Hospital of Huazhong University of Science and Technology and with the 1964 Helsinki declaration. Informed consent to participate in the study has been obtained from participants.

Consent for publication:

Not applicable.

Competing interests:

All authors report no conflicts of interest in this work.

References

1. Siegel RL, Miller KD, Jemal A. Cancer statistics. 2018. CA Cancer J Clin. 2018;68(1):7–30.
2. Linehan WM. Genetic basis of kidney cancer: role of genomics for the development of disease-based therapeutics. Genome Res. 2012;22(11):2089–100.
3. Barata PC, De Liano AG, Mendiratta P, Crolley V, Szabados B, Morrison L, et al. The efficacy of VEGFR TKI therapy after progression on immune combination therapy in metastatic renal cell carcinoma. Br J Cancer. 2018;119(2):160–3.
4. Lawrence MS, Stojanov P, Polak P, Kryukov GV, Cibulskis K, Sivachenko A, et al. Mutational heterogeneity in cancer and the search for new cancer-associated genes. Nature. 2013;499(7457):214–8.
5. Fridman WH, Zitvogel L, Sautes-Fridman C, Kroemer G. The immune contexture in cancer prognosis and treatment. Nat Rev Clin Oncol. 2017;14(12):717–34.
6. Kovacs SB, Miao EA. Gasdermins. Effectors of Pyroptosis. Trends Cell Biol. 2017;27(9):673–84.
7. Shi J, Zhao Y, Wang K, Shi X, Wang Y, Huang H, et al. Cleavage of GSDMD by inflammatory caspases determines pyroptotic cell death. Nature. 2015;526(7575):660–5.
8. Ding J, Wang K, Liu W, She Y, Sun Q, Shi J, et al. Pore-forming activity and structural autoinhibition of the gasdermin family. Nature. 2016;535(7610):111–6.
9. He WT, Wan H, Hu L, Chen P, Wang X, Huang Z, et al. Gasdermin D is an executor of pyroptosis and required for interleukin-1beta secretion. Cell Res. 2015;25(12):1285–98.
10. Rogers C, Erkes DA, Nardone A, Aplin AE, Fernandes-Alnemri T, Alnemri ES. Gasdermin pores permeabilize mitochondria to augment caspase-3 activation during apoptosis and inflammasome activation. Nat Commun. 2019;10(1):1689.
11. Kuang S, Zheng J, Yang H, Li S, Duan S, Shen Y, et al. Structure insight of GSDMD reveals the basis of GSDMD autoinhibition in cell pyroptosis. Proc Natl Acad Sci U S A. 2017;114(40):10642–7.
12. Liu Z, Wang C, Yang J, Zhou B, Yang R, Ramachandran R, et al. Crystal Structures of the Full-Length Murine and Human Gasdermin D Reveal Mechanisms of Autoinhibition, Lipid Binding, and Oligomerization. Immunity. 2019;51(1):43–9. e4.
13. Rogers C, Fernandes-Alnemri T, Mayes L, Alnemri D, Cingolani G, Alnemri ES. Cleavage of DFNA5 by caspase-3 during apoptosis mediates progression to secondary necrotic/pyroptotic cell death. Nat Commun. 2017;8:14128.
14. Fink SL, Cookson BT. Caspase-1-dependent pore formation during pyroptosis leads to osmotic lysis of infected host macrophages. Cell Microbiol. 2006;8(11):1812–25.
15. Qian BZ, Pollard JW. Macrophage diversity enhances tumor progression and metastasis. Cell. 2010;141(1):39–51.
16. Kolb R, Liu GH, Janowski AM, Sutterwala FS, Zhang W. Inflammasomes in cancer: a double-edged sword. Protein Cell. 2014;5(1):12–20.

17. Hou J, Zhao R, Xia W, Chang CW, You Y, Hsu JM, et al. PD-L1-mediated gasdermin C expression switches apoptosis to pyroptosis in cancer cells and facilitates tumour necrosis. Nat Cell Biol. 2020;22(10):1264–75.
18. Hergueta-Redondo M, Sarrio D, Molina-Crespo A, Megias D, Mota A, Rojo-Sebastian A, et al. Gasdermin-B promotes invasion and metastasis in breast cancer cells. PLoS One. 2014;9(3):e90099.
19. Miguchi M, Hinoi T, Shimomura M, Adachi T, Saito Y, Niitsu H, et al. Gasdermin C Is Upregulated by Inactivation of Transforming Growth Factor beta Receptor Type II in the Presence of Mutated Apc, Promoting Colorectal Cancer Proliferation. PLoS One. 2016;11(11):e0166422.
20. Karki R, Kanneganti TD. Diverging inflammasome signals in tumorigenesis and potential targeting. Nat Rev Cancer. 2019;19(4):197–214.
21. Xia X, Wang X, Cheng Z, Qin W, Lei L, Jiang J, et al. The role of pyroptosis in cancer: pro-cancer or pro-"host"? Cell Death Dis. 2019;10(9):650.
22. Man SM, Kanneganti TD. Regulation of inflammasome activation. Immunol Rev. 2015;265(1):6–21.
23. Ruhl S, Shkarina K, Demarco B, Heilig R, Santos JC, Broz P. ESCRT-dependent membrane repair negatively regulates pyroptosis downstream of GSDMD activation. Science. 2018;362(6417):956–60.
24. Hu L, Chen M, Chen X, Zhao C, Fang Z, Wang H, et al. Chemotherapy-induced pyroptosis is mediated by BAK/BAX-caspase-3-GSDME pathway and inhibited by 2-bromopalmitate. Cell Death Dis. 2020;11(4):281.
25. Zhou B, Zhang JY, Liu XS, Chen HZ, Ai YL, Cheng K, et al. Tom20 senses iron-activated ROS signaling to promote melanoma cell pyroptosis. Cell Res. 2018;28(12):1171–85.
26. Tan G, Huang C, Chen J, Zhi F. HMGB1 released from GSDME-mediated pyroptotic epithelial cells participates in the tumorigenesis of colitis-associated colorectal cancer through the ERK1/2 pathway. J Hematol Oncol. 2020;13(1):149.
27. Braun DA, Hou Y, Bakouny Z, Ficial M, Sant' Angelo M, Forman J, et al. Interplay of somatic alterations and immune infiltration modulates response to PD-1 blockade in advanced clear cell renal cell carcinoma. Nat Med. 2020;26(6):909–18.
28. Cookson BT, Brennan MA. Pro-inflammatory programmed cell death. Trends Microbiol. 2001;9(3):113–4.
29. Bergsbaken T, Fink SL, Cookson BT. Pyroptosis: host cell death and inflammation. Nat Rev Microbiol. 2009;7(2):99–109.
30. Kumari P, Russo AJ, Shivcharan S, Rathinam VA. AIM2 in health and disease: Inflammasome and beyond. Immunol Rev. 2020;297(1):83–95.
31. de Koning HD, van Vlijmen-Willems IM, Zeeuwen PL, Blokx WA, Schalkwijk J. Absent in Melanoma 2 is predominantly present in primary melanoma and primary squamous cell carcinoma, but largely absent in metastases of both tumors. J Am Acad Dermatol. 2014;71(5):1012–5.

32. Shah S, Qin S, Luo Y, Huang Y, Jing R, Shah JN, et al. AIM2 Inhibits BRAF-Mutant Colorectal Cancer Growth in a Caspase-1-Dependent Manner. Front Cell Dev Biol. 2021;9:588278.
33. Qi M, Dai D, Liu J, Li Z, Liang P, Wang Y, et al. AIM2 promotes the development of non-small cell lung cancer by modulating mitochondrial dynamics. Oncogene. 2020;39(13):2707–23.
34. Chen SL, Liu LL, Lu SX, Luo RZ, Wang CH, Wang H, et al. HBx-mediated decrease of AIM2 contributes to hepatocellular carcinoma metastasis. Mol Oncol. 2017;11(9):1225–40.
35. Panganiban RA, Sun M, Dahlin A, Park HR, Kan M, Himes BE, et al. A functional splice variant associated with decreased asthma risk abolishes the ability of gasdermin B to induce epithelial cell pyroptosis. J Allergy Clin Immunol. 2018;142(5):1469–78 e2.
36. Chen Q, Shi P, Wang Y, Zou D, Wu X, Wang D, et al. GSDMB promotes non-canonical pyroptosis by enhancing caspase-4 activity. J Mol Cell Biol. 2019;11(6):496–508.
37. Molina-Crespo A, Cadete A, Sarrio D, Gamez-Chiachio M, Martinez L, Chao K, et al. Intracellular Delivery of an Antibody Targeting Gasdermin-B Reduces HER2 Breast Cancer Aggressiveness. Clin Cancer Res. 2019;25(15):4846–58.
38. Komiyama H, Aoki A, Tanaka S, Maekawa H, Kato Y, Wada R, et al. Alu-derived cis-element regulates tumorigenesis-dependent gastric expression of GASDERMIN B (GSDMB). Genes Genet Syst. 2010;85(1):75–83.
39. Sun Q, Yang J, Xing G, Sun Q, Zhang L, He F. Expression of GSDML Associates with Tumor Progression in Uterine Cervix Cancer. Transl Oncol. 2008;1(2):73–83.
40. Zhou CB, Fang JY. The role of pyroptosis in gastrointestinal cancer and immune responses to intestinal microbial infection. Biochim Biophys Acta Rev Cancer. 2019;1872(1):1–10.
41. Ma X, Yang K, Lindblad P, Egevad L, Hemminki K. VHL gene alterations in renal cell carcinoma patients: novel hotspot or founder mutations and linkage disequilibrium. Oncogene. 2001;20(38):5393–400.
42. Hakimi AA, Voss MH, Kuo F, Sanchez A, Liu M, Nixon BG, et al. Transcriptomic Profiling of the Tumor Microenvironment Reveals Distinct Subgroups of Clear Cell Renal Cell Cancer: Data from a Randomized Phase III Trial. Cancer Discov. 2019;9(4):510–25.
43. Hah YS, Koo KC. Immunology and Immunotherapeutic Approaches for Advanced Renal Cell Carcinoma: A Comprehensive Review. Int J Mol Sci. 2021;22(9).
44. Senbabaoglu Y, Gejman RS, Winer AG, Liu M, Van Allen EM, de Velasco G, et al. Tumor immune microenvironment characterization in clear cell renal cell carcinoma identifies prognostic and immunotherapeutically relevant messenger RNA signatures. Genome Biol. 2016;17(1):231.

Figures

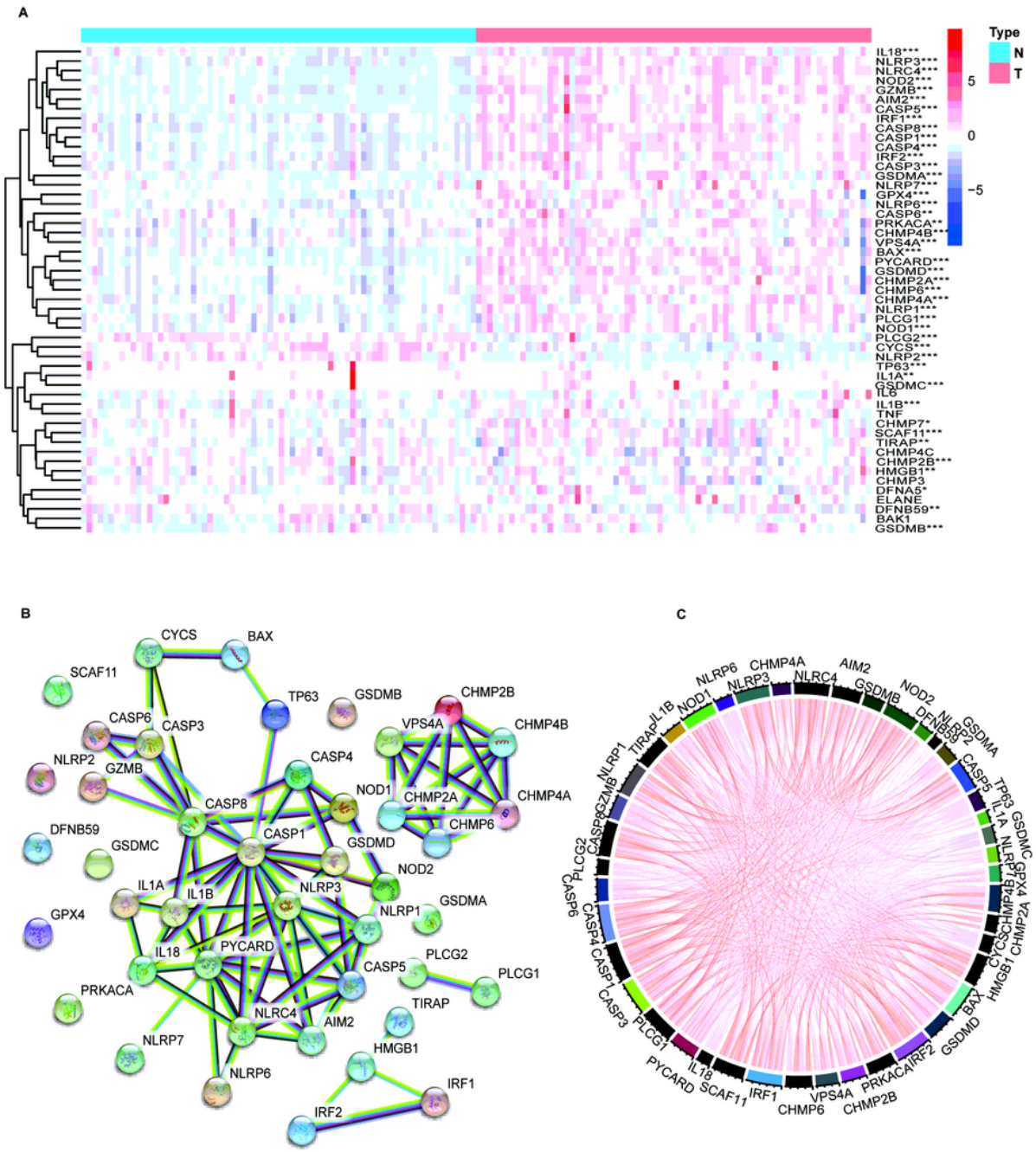

Figure 1

Expressions of the 41 pyroptosis-related genes and correlation chord diagram A Heatmap (blue: low expression levels; red: high expression level) of the pyroptosis-related genes in 71 tumour (T, red) and adjacent normal (N, blue) pairs. P values were showed as: *p <0.05, **p < 0.01, and ***p < 0.001. B PPI network showing the interactions of the pyroptosis-related genes (interaction score = 0.9). C The

correlation network of the pyroptosis-related genes (red line: positive correlation; blue line: negative correlation. The depth of the colors reflects the strength of the relevance).

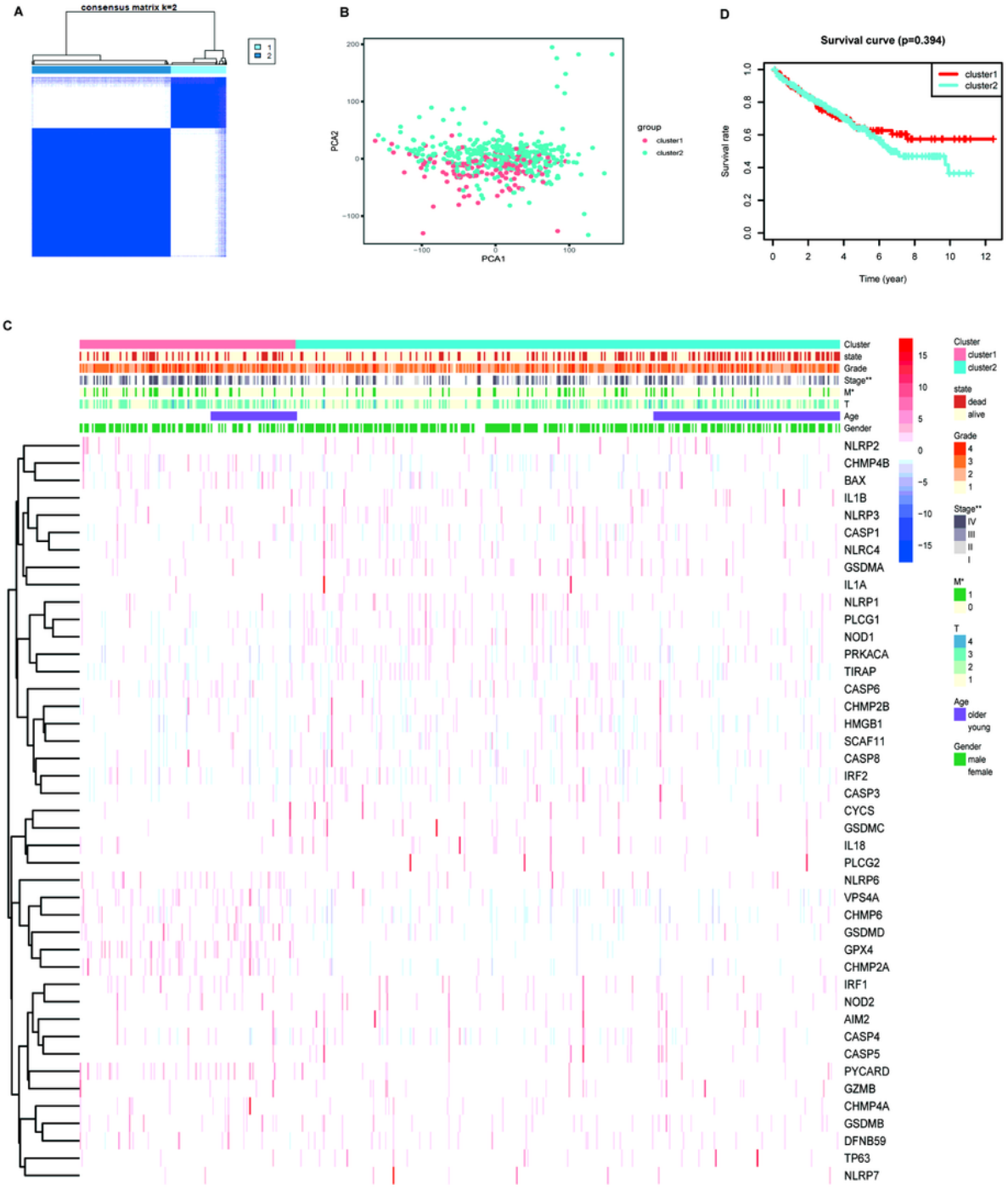

Figure 2

Cluster classification based on the pyroptosis-related DEGs A 494 ccRCC samples were grouped into two clusters according to the consensus clustering matrix (k = 2). B Principal component analysis (PCA) plot for ccRCC samples based on pyroptosis-related DEGs expression. Each point represents one sample, with

color indicating sample groups as described in the figure legend. C Heatmap and the clinicopathologic parameters of the two clusters classified by DEGs. P values were showed as: *p <0.05, **p < 0.01, and ***p < 0.001. D Kaplan–Meier OS curves for the two clusters.

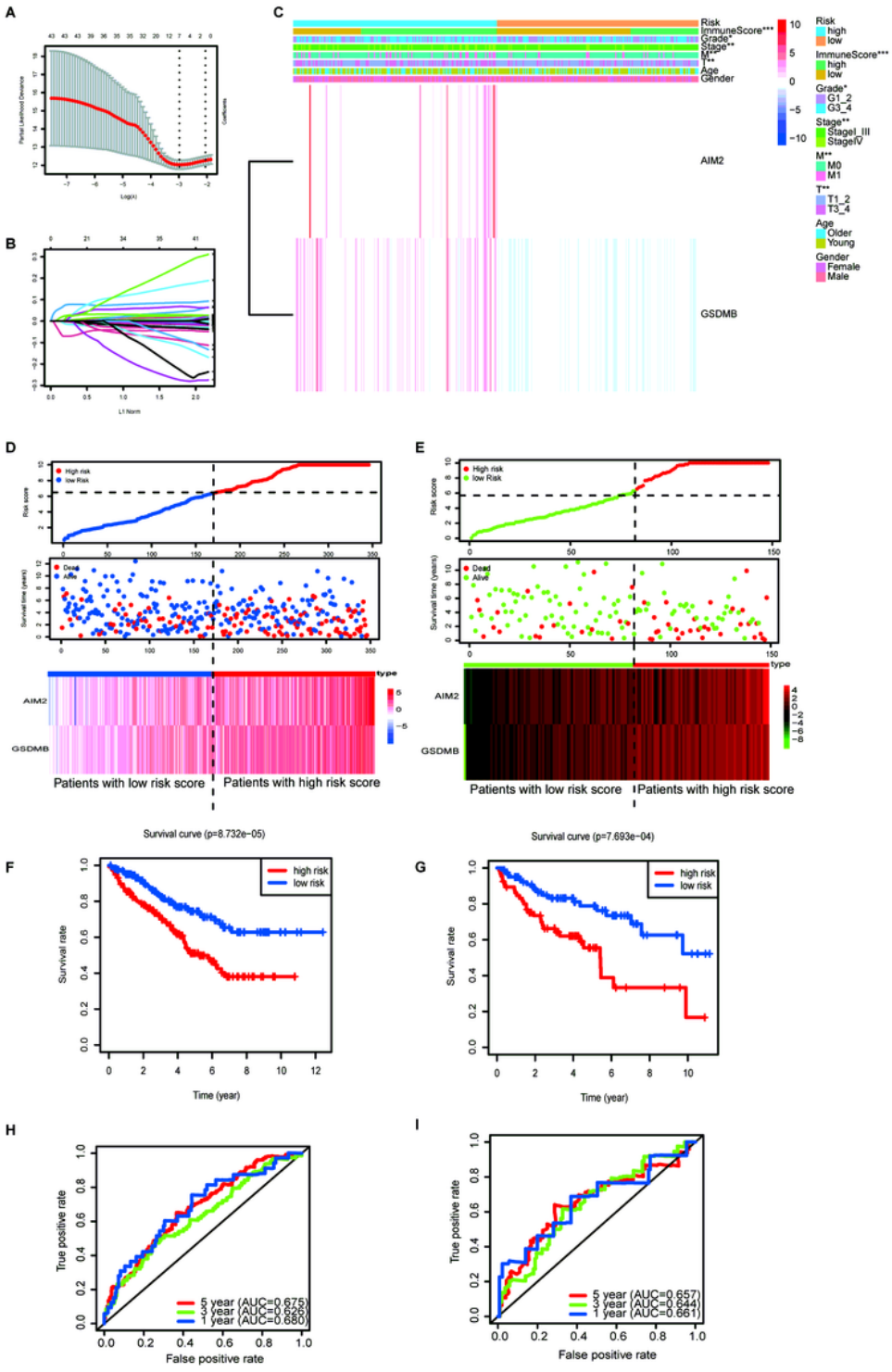

Figure 3

Construction of risk signature in the TCGA training cohort A-B Ten-fold cross-validation for tuning parameter selection in the LASSO model and the LASSO coefficient profiles of candidate genes are

shown. C Heatmap and clinicopathologic features of high- and low-risk subgroups. D-E The gene signature risk score, the vital status of patients and heatmap of the expression profiles of members in TCGA training and validation cohort. F-G Kaplan–Meier curves for the OS of patients in the high- and low-risk groups in TCGA training and validation cohort. H-I ROC curves plotted for 1-, 3- and 5-y overall survival in TCGA training and validation cohort.

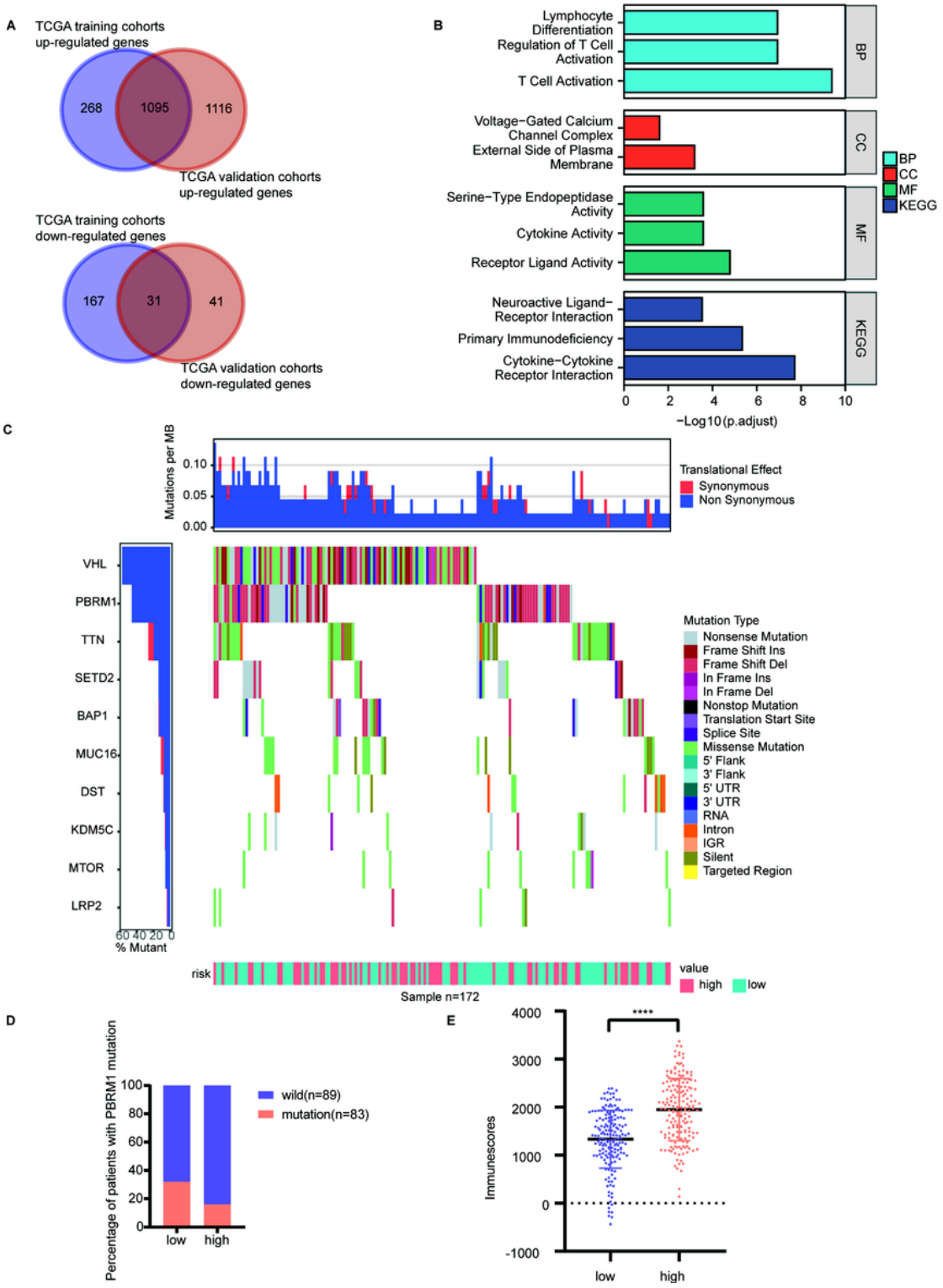

Figure 4

Functional analysis based on the DEGs between the two-risk groups in TCGA cohort. A Overlapped DEGs in TCGA training and validation cohort B GO and KEGG analyses of DEGs and terms are shown on the left C The mutation frequency in the TCGA training cohort. D Percentange of PBRM1 mutation in the TCGA training cohort. E Immunoscore in the high and low subgroups. P values were showed as: *p <0.05, **p < 0.01, and ***p < 0.001.

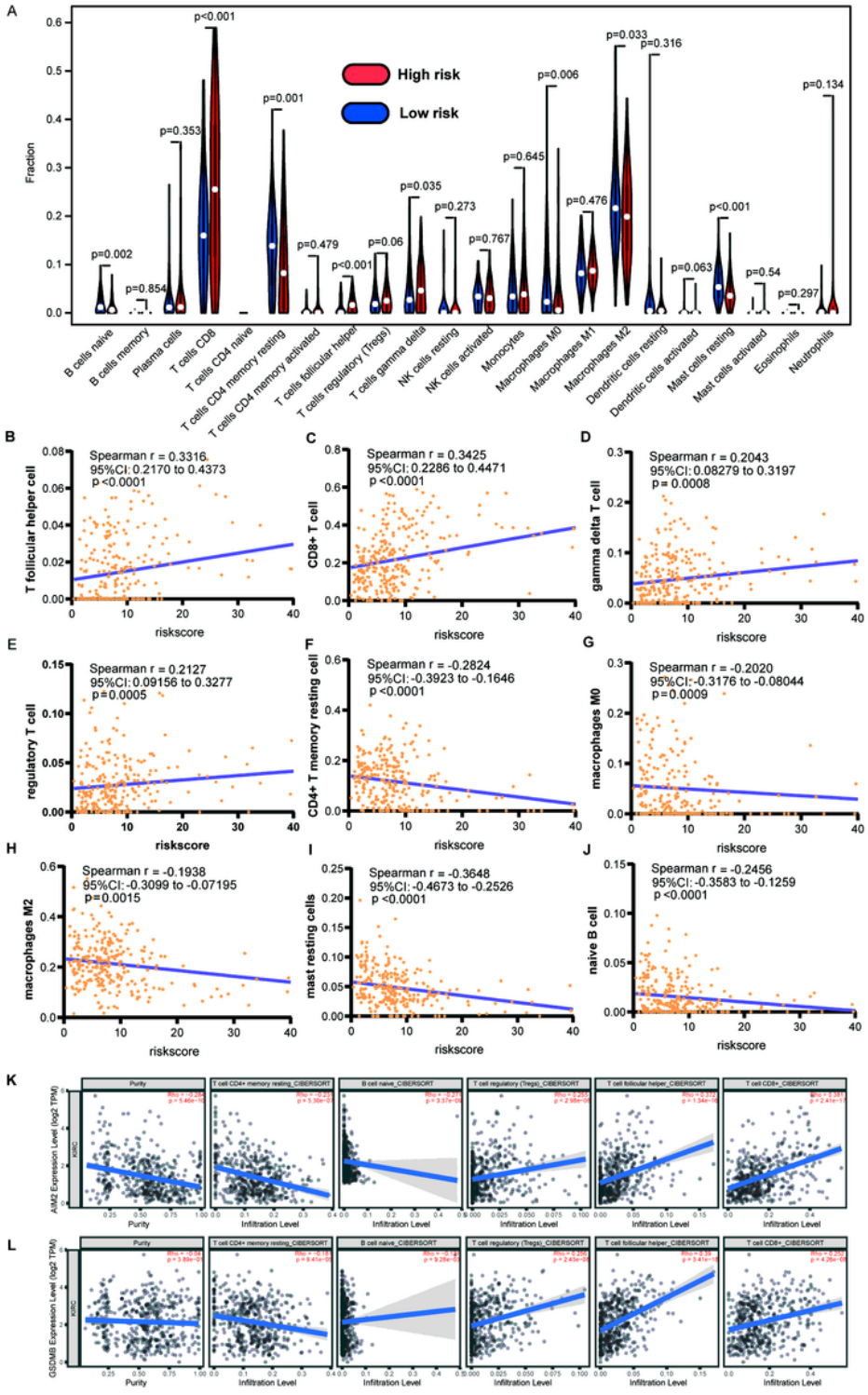

Figure 5

Relationships between the risk score and infiltration abundances of nine immune cell types A Violin plot of the relative infiltration level of immune cells in the TCGA training cohort B-J T follicular helper cell (B), CD8+ T cell (C), gamma delta T cell (D), regulatory T cell (E), CD4+ T memory resting cell (F), macrophages M0 (G), macrophages M2 (H), mast resting cells (I), and naive B cell (J). K AIM2 expression is significantly negatively related to tumour purity and has significant positive correlations with infiltrating levels of regulatory T, T follicular helper, CD8+ T cells, and negative correlations with CD4+ T memory resting, naive B cells. L GSDMB expression also has significant positive correlations with infiltrating levels of regulatory T, T follicular helper, CD8+ T cells, and negative correlations with CD4+ T memory resting, naive B cells in ccRCC.

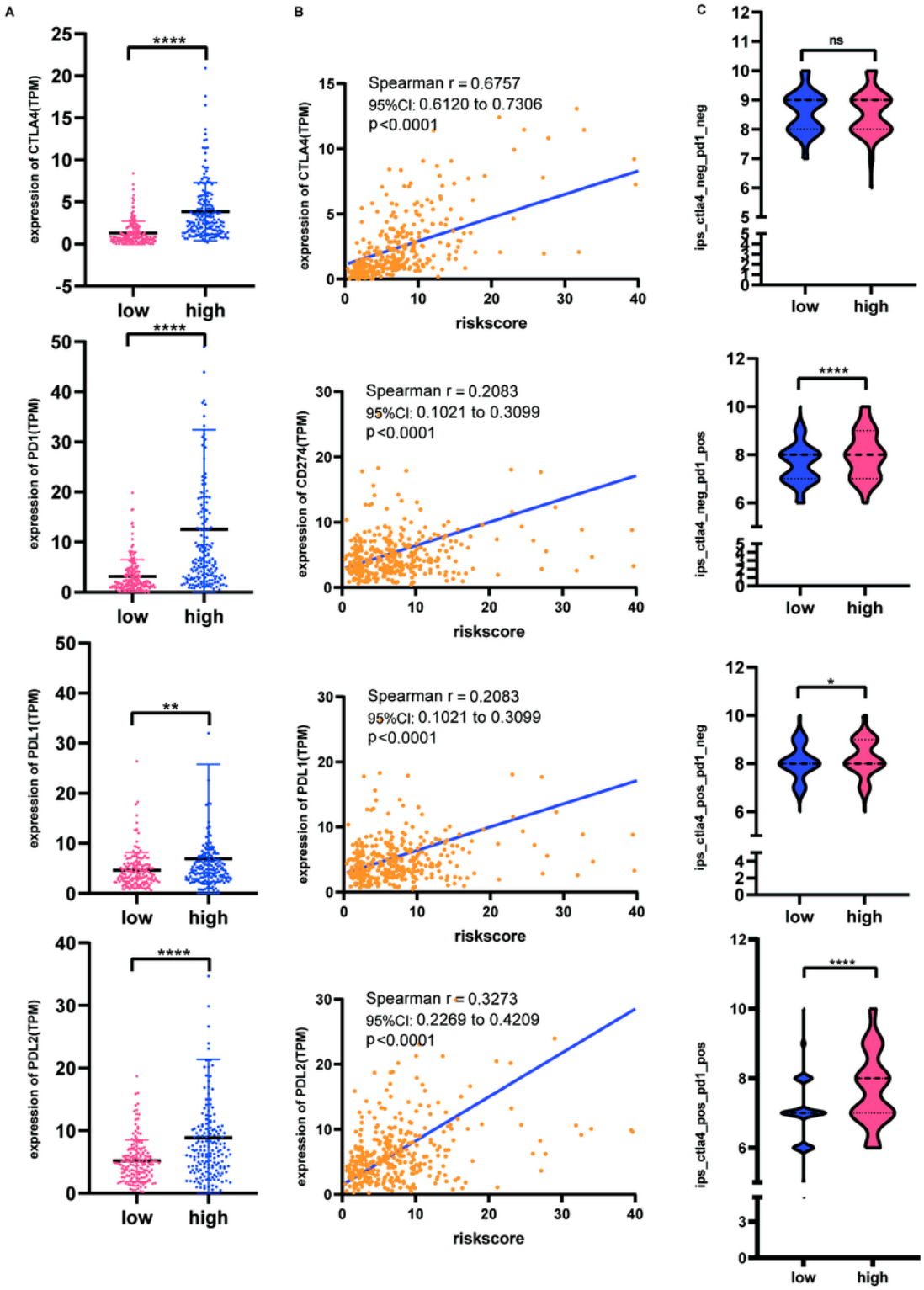

Figure 6

The estimation of two risk score subtypes in immunotherapy response. A The expression of 4 immune checkpoint molecules (CTLA4, PD1, PD-L1 and PDL2) in two prognostic subtypes. B The spearman correlation coefficient calculated between risk score and 4 immune checkpoint molecules. C The associations between IPS and risk score. P values were showed as: ns means no significance, *p <0.05, **p < 0.01, and ***p < 0.001.

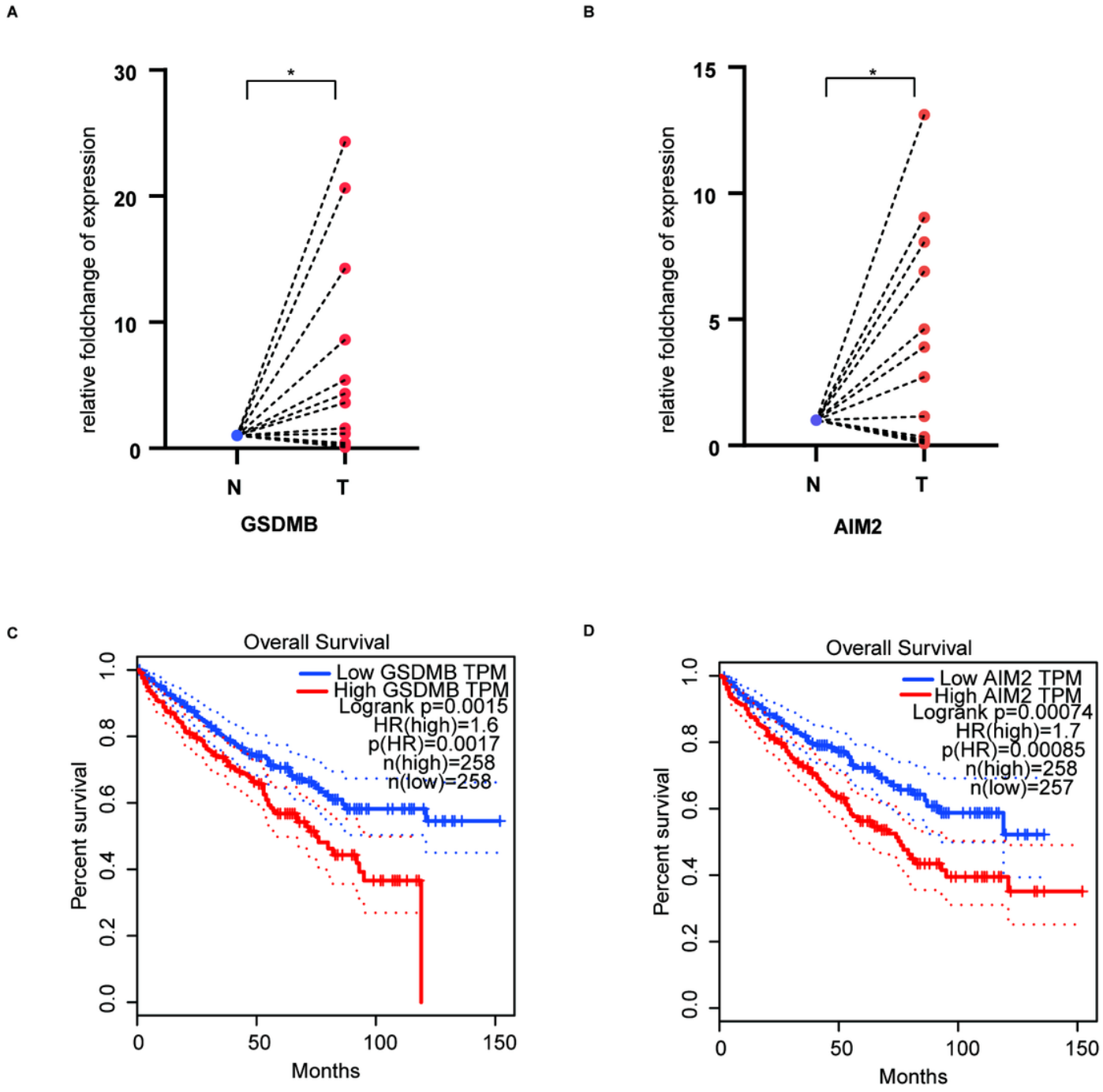

Figure 7

AIM2 and GSDMB are upregulated in ccRCC tissues and are correlated with worse prognosis A-B The mRNA expression level of AIM2 and GSDMB was upregulated in ccRCC tissues. P values were showed as: *p <0.05, **p < 0.01, and ***p < 0.001. C-D OS was analysed according to high or low expression of AIM2/GSDMB and log-rank t test was used

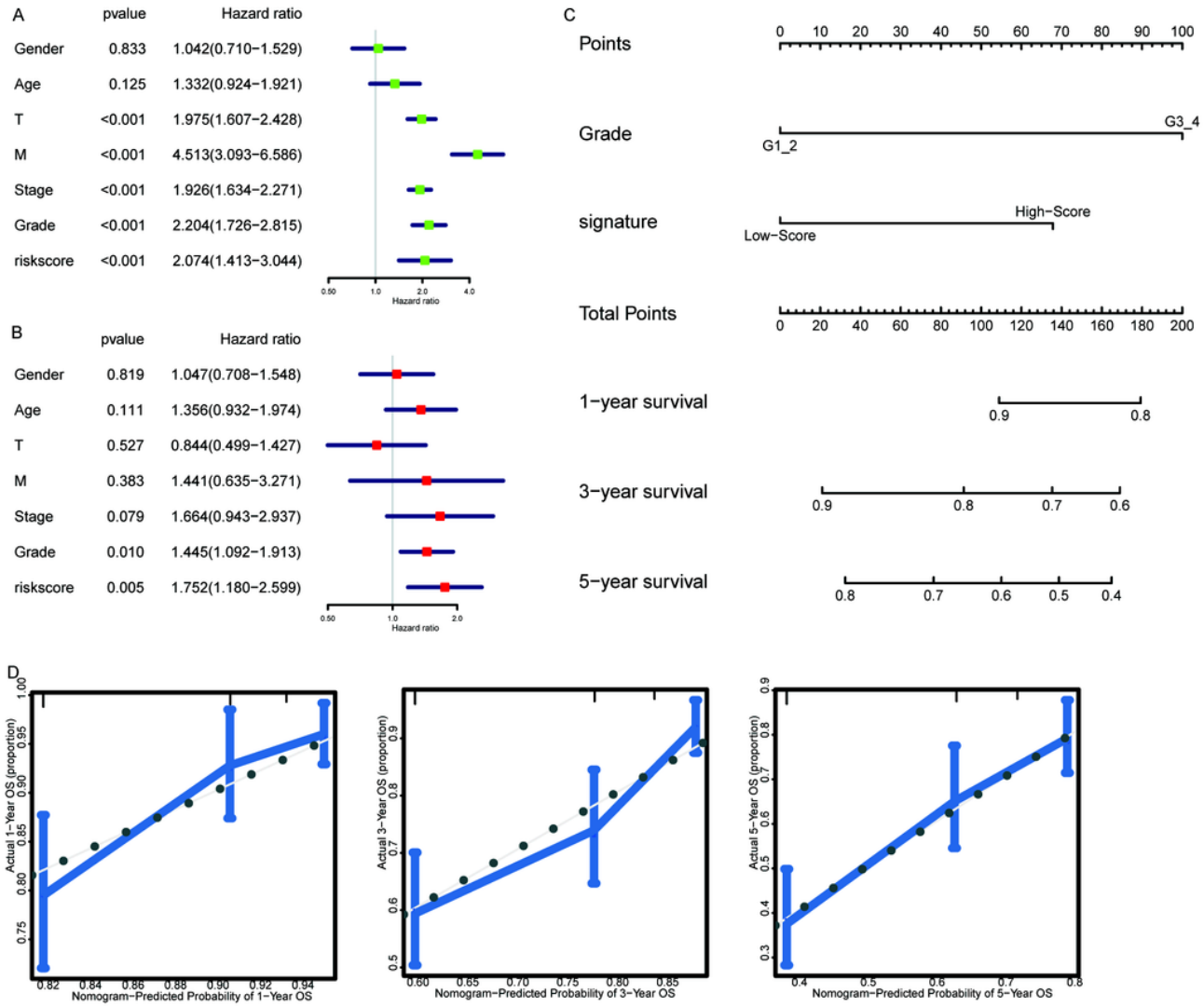

Figure 8

Nomogram for predicting the probability of OS in ccRCC patients A-B Univariate analysis and multivariate analysis containing risk score and clinical characteristics. C A nomogram for predicting OS in patients with ccRCC D Calibration plot of the nomogram for the probability of OS at 1, 3 and 5 y.

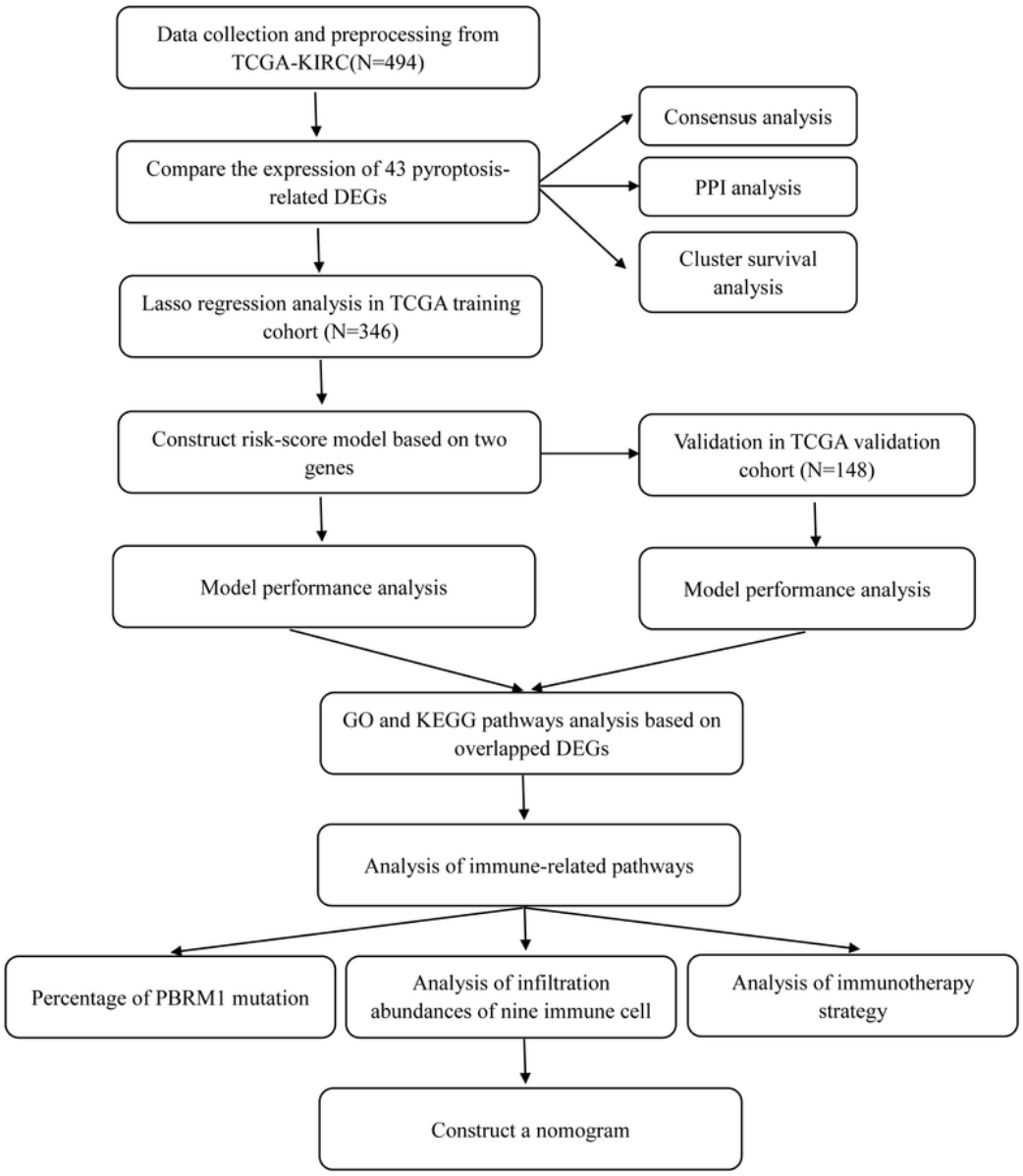

Figure 9

Analysis workflow

Supplementary Files

This is a list of supplementary files associated with this preprint. Click to download.

- AdditionalFile1TableS1.xlsx
- AdditionalFile2TableS2.xlsx
- AdditionalFile3TableS3.xlsx
- AdditionalFile4TableS4.xlsx
- AdditionalFile5FigS1.tif